Available online at www.sciencedirect.com
SCIENCE DIRECT®
International Journal of Fatigue 26 (2004) 691–703
International Journal of Fatigue
www.elsevier.com/locate/ijfatigue

Effect of temper, specimen orientation and test temperature on tensile and fatigue properties of wrought and PM AA6061-alloys

J.C. Huang [a], C.S. Shin [a,*], S.L.I. Chan [b]

[a] Department of Mechanical Engineering, National Taiwan University, No. 1, Sec. 4, Roosevelt Road, Taipei, Taiwan, ROC
[b] Department of Materials Science and Engineering, National Taiwan University, No. 1, Sec. 4, Roosevelt Road, Taipei, Taiwan, ROC

Received 24 April 2003; received in revised form 18 July 2003; accepted 20 November 2003

Abstract

The tensile and fatigue crack growth properties of 6061 Al alloy fabricated by powder metallurgy (PM) and ingot metallurgy (IM) routes have been evaluated at temperatures ranging from 25 to 300 °C. At 25 °C, the PM alloy possesses a higher strength, higher strain hardening rate and a lower elongation than the IM alloy. Raising the testing temperature from 25 to 200 °C greatly reduced the advantage in strength of the PM alloy over that of the IM alloy. At 300 °C, both alloys possess similar strength. The fatigue crack growth resistance in the TL orientation is inferior to that in the LT orientation for both alloys in T4 and T6 tempers. The difference in resistance is evident at low stress intensity in the IM alloy and is believed to be resulted from the interaction between grain size and plastic zone size, and at high stress intensity in the PM alloy which is attributable to the difference in fracture toughness. The difference in crack growth resistance between the two orientations decreases with increasing temperature and is basically non-existent at 300 °C. Furthermore, the fatigue crack growth resistance in the T6 temper is superior to that in the T4 temper. In both alloys, fatigue crack growth resistance decreases with increasing temperature. Such decrease is more prominent from 25 to 200 °C and from 250 to 300 °C. At all temperatures, the PM alloy always has an inferior crack growth resistance as compared to the IM alloy.

Keywords: Fatigue crack growth; Temperature; Orientation; PM; Plastic zone size

1. Introduction

When compared with structural steels, aluminum alloys [1,2] have much better specific strength and corrosion resistance. However, a major drawback of aluminum alloys is the rapid loss of strength at elevated temperatures [3–6]. One way to combat this is to add ceramic particles such as silicon carbide (SiC) [7–13] to produce aluminum-based metal matrix composites (AMMC). This will raise the strength, stiffness, wear resistance and increase the usable temperature range of the alloys [14–17]. One route to produce AMMC is through the powder metallurgy (PM) method [18].

Investigations on elevated temperature fatigue crack propagation (FCP) behaviors of Al alloys are still limited [19–21], especially for PM materials at temperature near 300 °C, where β′ phase started to form [22–24]. Blankenship and Kaisand [19] studied the FCP behavior of the ingot metallurgy (IM) 2095 Al and compared the fracture surface morphology between 25 and 175 °C. Healy and Beevers [25] studied the FCP behaviors of spray deposited 2618 Al at 180 °C. They found that increasing the temperature to 180 °C resulted in lower threshold values and increased fatigue crack growth rates. Tanaka et al. [26] studied the FCP behaviors of the IM 6061 Al at 170 and 280 °C. They found that fatigue crack growth rates increase with an increase in temperature. A higher degree of crack closure occurred at lower temperatures. However, under the same ΔK_{eff}, fatigue cracks were found to grow at low rates at higher temperatures. Bray [21] studied the FCP behaviors of the dispersion-strengthened PM aluminum alloys at 225 °C. He showed that resistance of the PM alloys was less due to a paucity of crack tip

* Corresponding author. Tel./fax: +886-2-2362-2160.
E-mail address: csshin@ccms.ntu.edu.tw (C.S. Shin).

0142-1123/$ - see front matter © 2003 Elsevier Ltd. All rights reserved.
doi:10.1016/j.ijfatigue.2003.11.006

shielding mechanisms and the crack growth rates increased with decreasing frequency as a result of environmental effects.

A series of work have been undertaken to evaluate the elevated temperature properties of SiC reinforced 6061 alloy made by the PM route. To shed more light on the understanding of the elevated temperature behavior of AMMC, preliminary work to compare the tensile and fatigue properties at elevated temperatures of the basic aluminum alloy produced by PM with that of the IM alloy was carried out first and will be reported in this paper.

2. Experimental procedure

2.1. Preparation of the 6061 alloys

Commercial grade T6-IM-6061 aluminum alloy plate of thickness 6.35 mm was purchased, while PM 6061 alloy was manufactured in our laboratory from air-atomized aluminum powder. The powder was of irregular shape with a mean "diameter" of 122 μm. After thorough blending, the powder was compacted to a round billet of 80 mm diameter using cold isostatic pressing at 300 MPa. The billet was then degassed at 450 °C for 2 h and sintered with partial liquid phase at 600 °C for 2 h. After sintering, the 80 mm diameter billet was further compacted by hot extrusion at 470 °C to a plate with a cross-section of 40 mm × 8 mm. The density of the extruded plate is above 99% of the theoretical density. Table 1 shows the chemical composition of the present PM and IM 6061 alloys in weight percent. The IM alloy has a much higher Fe and Cr contents, but slightly less amount of Mg and Si than the PM alloy.

Standard tensile and compact tension specimens were machined from both alloys. Tensile specimens of 100 mm long and 6 mm thick, with a gage length of 30 mm were machined conforming to ASTM B557M-84. The compact tension specimens conformed to ASTM E647 and measured 31.2 × 32.5 × 6 mm. Compact tension specimens were machined in both the LT and TL orientations.

After machining, all specimens were solution heat treated at 540 °C for 2 h. Half of the specimens were then naturally aged (T4) at room temperature for 60 days. The other half was peak aged (T6) at 160 ± 1 °C for 20 h in an oil-bath furnace. Fig. 1 shows the variation of hardness as a function of aging time for the PM and IM 6061 Al alloys. For the PM alloy, peak hardness was reached after aging at 160 °C for 20 h. Thereafter, hardness dropped abruptly at first and remained at a more or less stable value up to about 100 h. For the IM alloy, although the peak hardness was reached at about 50 h, the rate of increase in hardness slowed down abruptly after about 20 h and stayed more or less at a plateau value up to 100 h. Hence aging at 160 °C for 20 h was chosen for the T6 temper of both PM and IM alloy specimens.

Table 1
Chemical compositions of PM and IM 6061 alloys (wt%)

	Mg	Si	Cu	Fe	Cr	Mn	Ti	Al
PM	0.96	0.60	0.35	0.12	0	0	0	Bal.
IM	0.92	0.54	0.25	0.46	0.22	0.05	0.02	Bal.

2.2. Tensile and fatigue crack propagation tests

Both types of tests were conducted using a MTS 810 servo hydraulic testing machine. Tensile tests were carried out according to ASTM B557M. For room temperature testing, a strain-gage-based extensometer was used for monitoring strain. For high temperature testing, the specimens in suitable grips were enclosed in a furnace where temperature could be controlled to within ±1 °C. Temperature was raised at 2–3 °C per minute and the specimens were kept at the desired temperature for 30 min before testing commenced. A microscope equipped with image processing software was used to measure the change in gage length. Elevated temperature tensile tests were carried out at 200 and 300 °C on specimens with T6 treatment only.

Fatigue crack propagation was carried out with constant amplitude sinusoidal loading at 20 Hz with a stress ratio ($R = K_{min}/K_{max}$) of 0.1. Crack length was monitored by a travelling microscope at a resolution of 0.01 mm. Elevated temperature fatigue tests were carried out at 200, 250 and 300 °C. The same temperature raising and preheating procedure as that for tensile tests was employed. Preheating and testing at elevated

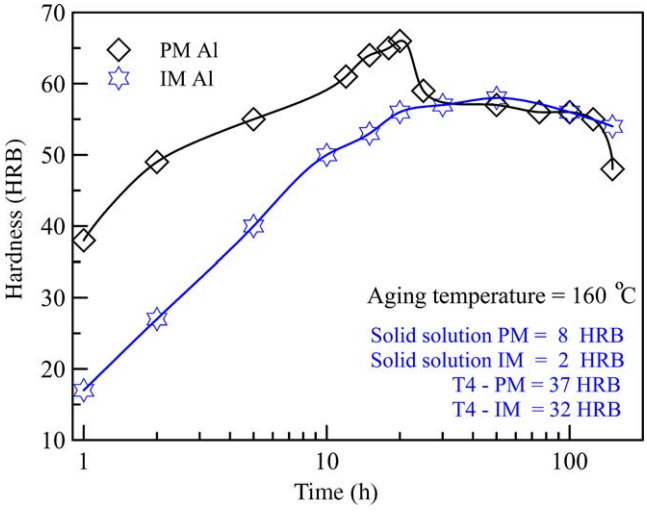

Fig. 1. The variation of hardness with aging time for the PM and IM 6061 Al alloys.

temperatures would induce additional precipitation and changes in hardness. Fig. 2 compares the hardness of the specimens before testing, after soaking for 30, 180 min and after fatigue testing at different testing temperatures. At 200 °C, the specimens exhibited less than 10% drop in hardness even under prolonged fatigue testing. At 250 °C and higher, both alloys exhibited significant aging softening. Although softening after fatigue testing is the most serious, the incremental drop in hardness from 180 min up to the end of fatigue testing is not significant. In order to gain more understanding on the crack propagation mechanisms, the development of crack closure had also been monitored by a compliance method with offset procedure using a back face strain gage. The stress intensity level corresponding to the turning point on the offset compliance curve is denoted as the crack closure intensity (K_{cl}). The degree of crack closure, U, was defined as the fraction of the load range for which the crack is open

$$U = (K_{max} - K_{cl})/(K_{max} - K_{min}) = \Delta K_{eff}/\Delta K \quad (1)$$

ΔK_{eff} is the effective range of stress intensity available for growing a crack. The frequency was reduced to 0.5 Hz during the measurement of crack closure.

The microstructure was observed by optical micro scopy (OM) and transmission electron microscopy (TEM). For TEM observation, thin disk-shaped foils parallel and perpendicular to the rolling or extrusion plane were prepared by machining and twin-jet polishing apparatus using a 25% HNO_3 + 75% methanol solution at −30 °C and a potential difference of 10–14 V. Fracture surfaces of the specimens were examined with a scanning electron microscope (SEM).

3. Results and discussion

3.1. Tensile properties

3.1.1. Room temperature tensile properties

Fig. 3 compares the room temperature tensile properties of the PM and IM alloys in the T4 and T6 conditions. As expected, in both alloys, the T6 temper produced higher strength and lower elongation than the T4 temper. Under the same heat treatment condition, the PM alloy always possessed a higher strength, a higher strain hardening rate and a lower elongation than the IM alloy. This may be attributed to the smaller grain size of the PM alloy. Fig. 4 compares the microstructure of the PM and IM alloys. Average grain size for the PM alloy was $4 \times 2 \times 5$ μm, while those for the wrought alloy was $200 \times 100 \times 300$ μm. The smaller grain size in the PM alloy resulted from recrystallization that occurred during sintering and during hot extrusion [27–29]. TEM micrographs (Fig. 5) show the interaction of dislocations and dispersoids in T4-IM alloy, morphology of the large constituent particle and the fine dispersoids in T6-IM alloy, and the elongated grain in the extruded direction in the PM alloy.

Typical tensile fracture surfaces show that both the IM and PM alloys in T4 and T6 tempers failed by the coalescence of microvoids. In IM, the fracture surface consisted of mainly large dimple voids, while in the PM, there are numerous smaller microvoids interspersed among the large dimple voids. EDAX analysis showed that the constituents inside the large dimple voids were FeSiAl particles [30,31] in all four cases. For the smaller microvoids on the PM fracture surfaces, EDAX analysis aimed inside the voids showed essentially the same results as that at the base metal, except that the oxygen content was higher. Thus, the

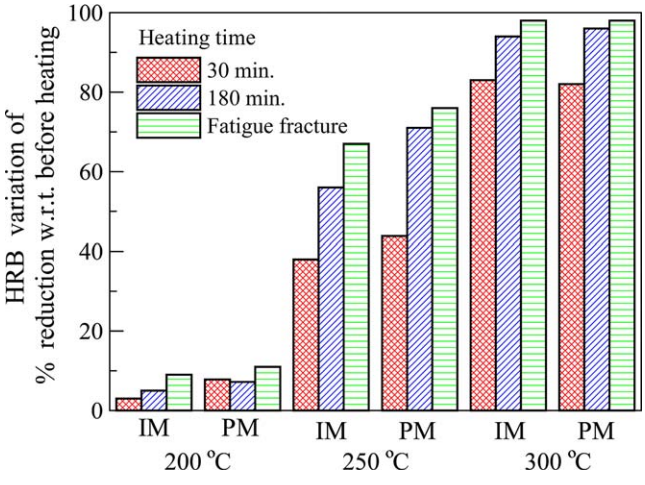

Fig. 2. Comparison of hardness change after pre-heating/soaking and fatigue testing at various temperatures for the PM and IM 6061 Al alloys.

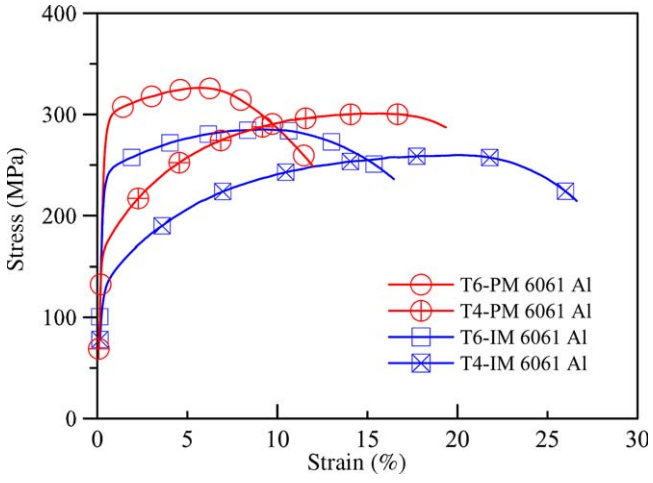

Fig. 3. Room temperature stress–strain curves of PM and IM 6061 Al alloys in the T4 and T6 tempers.

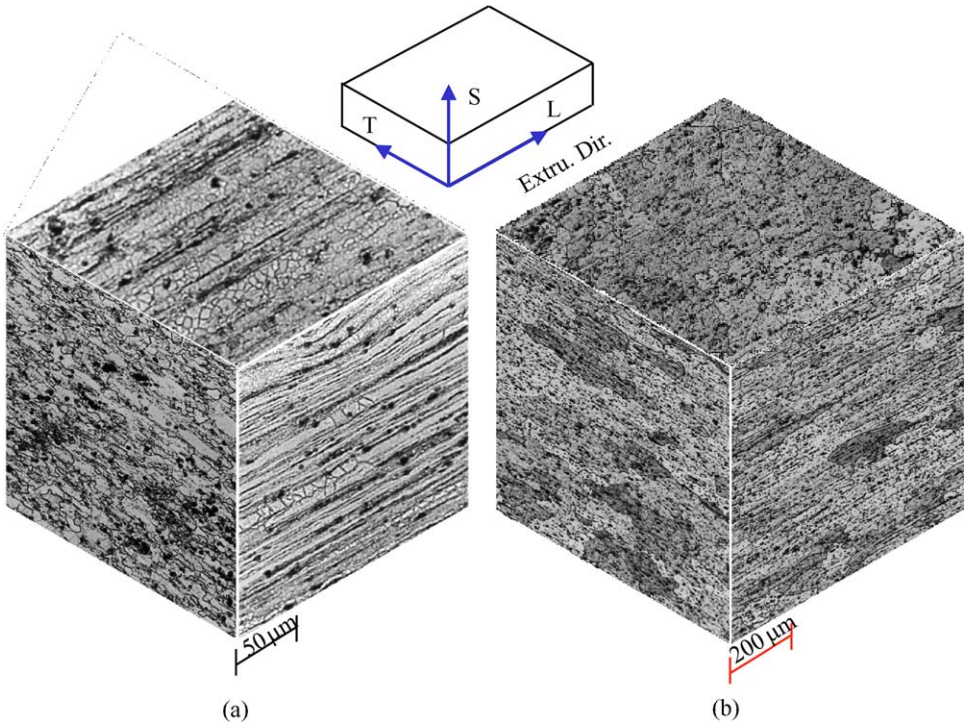

Fig. 4. Three-dimensional optical microstructure of the etched (a) PM and (b) IM 6061 Al alloy in the T6 heat treatment.

particles inside these smaller microvoids were probably alumina. The T4 treatment produced fewer and more coherent precipitates than the T6 treatment. During plastic deformation, the nucleation of microvoids will be delayed and this may be the reason that the T4 alloy has a much larger strain at fracture than the T6 alloy. Regarding the PM alloy, a thin layer of oxide invariably existed on the outside surface of the original aluminum powder. During extrusion, this layer was crushed and dispersed along the prior powder boundaries (see the TEM micrograph in Fig. 5b). These alumina particles together with the more numerous grain boundaries, do promote nucleation of microvoids at the fast coalescence stage and so the PM alloy has an earlier void nucleation and lower strain at fracture than the IM alloy.

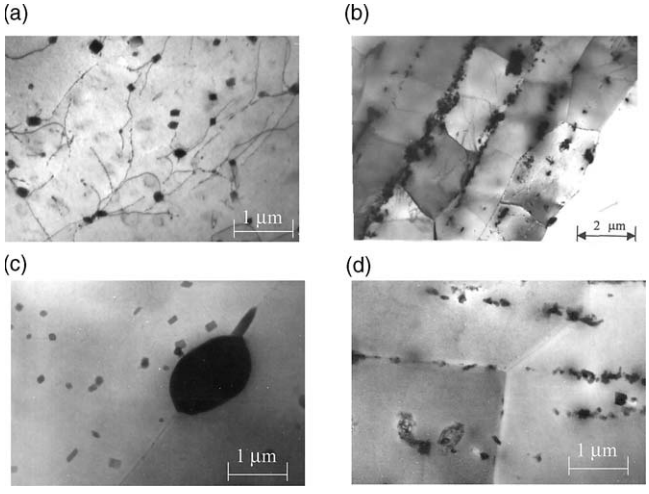

Fig. 5. Transmission electron micrograph showing (a) T4-IM, fine dispersoids pinned dislocation, T4-IM −25 °C, 20000× (b) T6-PM, alumina particles dispersed along prior powder boundary, T6-PM −25 °C, 8000× (c) T6-IM, larger constituent and fine dispersoids, T6-IM −25 °C, 20000× (d) T6-PM, alumina on grain boundary and within grain, T6-PM −25 °C, 20000×.

3.1.2. Elevated temperature tensile properties

As the testing temperature is raised, all the precipitates will grow and coarsen. Thus the morphology, size, and shape of the precipitates will deeply depend on time and temperature [32,33]. Fig. 6 compares the morphology and density of precipitates. The morphology and size of the precipitates are similar in both alloys. Using the method suggested by Andersen et al. [22], the number densities of the precipitate in both alloys are estimated to be about $2 \times 10^6/\mu m^3$, $6 \times 10^3/\mu m^3$ and $6 \times 10^2/\mu m^3$ at 25, 200 and 300 °C, respectively. A higher precipitate number density offers more resistance to dislocation movement and yields a higher strength and smaller fracture strain. Fig. 7 compares the tensile curves of the T6-IM and T6-PM alloys at three different temperatures. The advantage in strength of the PM alloy over that of the IM alloy was greatly reduced at 200 °C and became nearly non-existent at 300 °C. Table 2 shows the yield strength and

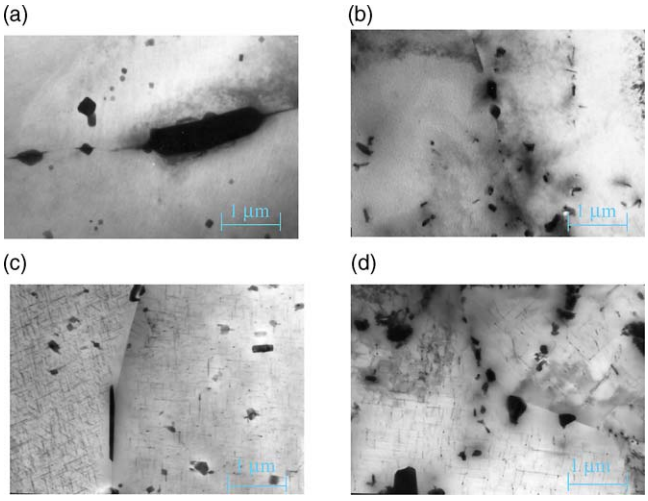

Fig. 6. Transmission electron micrograph showing fine needle precipitates and coarse rod precipitates and precipitate free zones in both alloys under 200 and 300 °C. (a) T6-IM −200 °C, 20000× (b) T6-PM −200 °C, 20000× (c) T6-IM −300 °C, 20000× (d) T6-PM −300 °C, 20000×

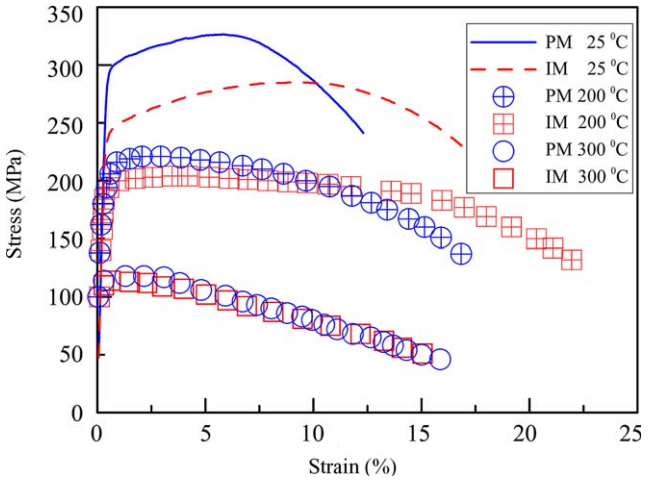

Fig. 7. Stress–strain curves of PM and IM 6061 Al alloys under different temperatures.

elongation of the alloys for the various conditions. Using the respective room temperature properties as the reference, the decrease in yield strength and tensile strength was comparably more pronounced in the PM alloy than in the IM alloy at both elevated temperatures (see Fig. 8). Raising the temperature to 200 °C

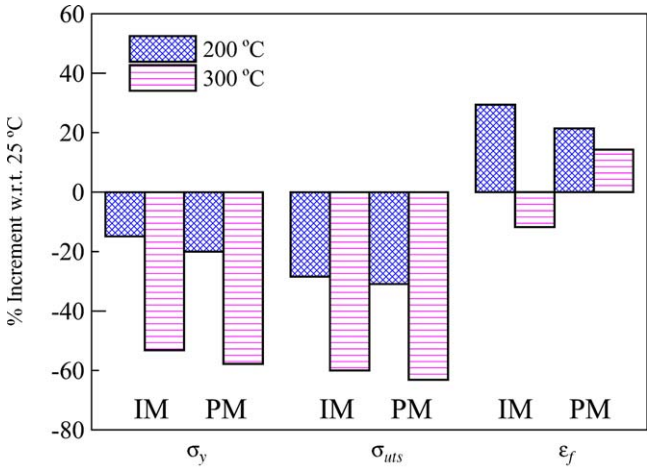

Fig. 8. Comparison of percentage change in elevated temperatures σ_y, σ_{uts} and ε_f of T6 PM and IM 6061 Al alloys with respect to that at 25 °C.

increased the strain at fracture more in the IM alloy. However, when the temperature was further raised to 300 °C, the yield strength and strain at fracture in both alloys decreased. In the IM alloy, the decrease was so marked that its elongation was below the room temperature level. Macroscopically, all samples but the IM alloy at 300 °C showed pronounced necking and cup-and-cone fracture. The IM alloy at 300 °C only showed slight necking. From the lack of necking and the shape of the tensile curve, it may be reasoned that there is little strain hardening occurring in the IM alloy at 300 °C.

3.2. Fatigue crack propagation properties

3.2.1. Effect of specimen orientation

Fig. 9a and b compares the room temperature fatigue crack growth rate versus ΔK for the IM and PM alloys in both the LT and TL orientations in the T4 and T6 tempers. For both tempers, the LT orientation offered slightly better fatigue crack growth resistance than the TL orientation. This difference tends to be more marked in the IM alloy at low stress intensity ranges and can in part be explained by the hindering effect of the grain boundary on cyclic slip as follows: the monotonic plane strain plastic zone size at $K_{max} =$ 6.6 MPa$\sqrt{m}$ (corresponding to a $\Delta K = 6$ MPa$\sqrt{m}$) as

Table 2
Yield strength and strain-to-fracture for the PM and IM alloys tested under different conditions

	T4—25 °C		T6—25 °C		T6—200 °C		T6—300 °C	
	σ_y (MPa)	ε_f (%)	σ_y (MPa)	ε_f (%)	σ_y (MPa)	ε_f (%)	σ_y (MPa)	ε_f (%)
PM	175	18	270	14	225	17	110	16
IM	122	28	235	17	200	22	105	15

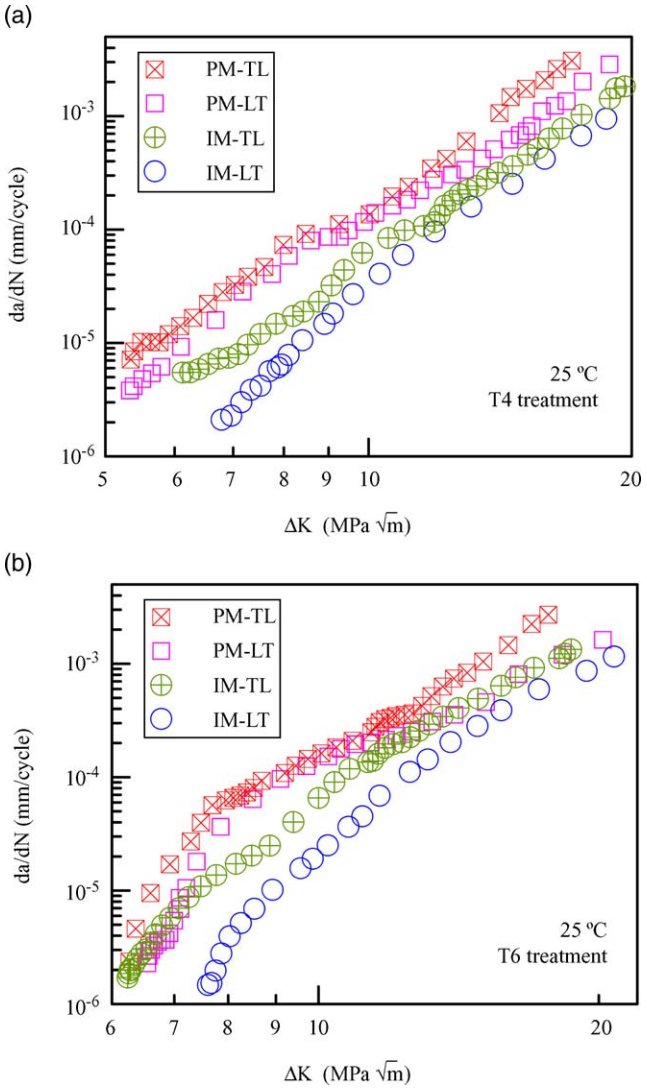

Fig. 9. Comparison of da/dN versus ΔK for the IM and PM alloys in both the LT and TL orientations under the (a) T4 and (b) T6 treatment at room temperature.

estimated by Irwin's model [34] is 80 μm in the T6-IM alloy. This is smaller than the grain dimensions in the L (300 μm) and T (200 μm) directions. Both T4 and T6 treatment conditions have the same grain dimensions. In the T4-IM alloy, owing to a lower strength, the plastic zone size (320 μm) is roughly equal to the grain dimension in the L direction. On the other hand, at the same stress intensity range, the plastic zones in the PM alloy in either the T4 (150 μm) or T6 (60 μm) conditions spanned a considerable number of grains ($4 \times 2 \times 5$ μm). At higher temperatures, the above effect of plastic zone versus grain size is diminishing due to a significant drop in yield strength and to grain refinement by partial recrystallization. Incidentally, the difference in fatigue crack growth resistance nearly vanished (see Fig. 10a–c).

The marked difference (see Figs. 9 and 10) in growth rate at high intensity levels in the PM may be explained in terms of the anisotropy in fracture toughness. The respective fracture toughness was estimated by loading the specimens statically to fracture after fatigue testing to a crack length of 16 mm. The estimated fracture toughnesses of the T6-IM alloys in LT and TL orientations are roughly equal to 30.2 and 26.9 MPa$\sqrt{\text{m}}$ at 25 °C, while that for the T6-PM alloys are 29.1 and 22.1 MPa$\sqrt{\text{m}}$, respectively. Thus, at the high stress intensity level where difference in growth rate became marked, the maximum stress intensity of the T6-PM-TL specimen is close to its fracture toughness, while that of the LT specimen is still below its respective fracture toughness level. The same comparison is not so prominent in the IM alloy as the fracture toughness values are closer together. As the testing temperature is raised, difference in the fracture toughness between the LT and TL orientations is decreased. At 300 °C, the fracture toughness decreased to about the same value of 15 MPa$\sqrt{\text{m}}$ in all four cases. Incidentally, the difference in fatigue crack growth resistance between the LT and TL orientations at 300 °C nearly vanished (Fig. 10c).

3.2.2. *Effect of heat treatment*

Fig. 11a compares the fatigue crack growth behavior of the PM and IM alloys in the T4 and T6 tempers in the LT orientation. The crack growth rate in PM is higher than that in IM for the same ΔK. In general, the difference in fatigue crack growth between IM and PM alloys is more marked than that between T4 and T6 tempers of the same alloy. Furthermore, the difference between the T4 and T6 tempers is only significant at low ΔK levels, which are 8 MPa$\sqrt{\text{m}}$ in the PM alloys and 11 MPa$\sqrt{\text{m}}$ for the IM alloys. For higher ΔKs, the crack growth rates versus ΔK behavior of the same alloy under the two heat treatment conditions are nearly the same. On the other hand, the crack closure behavior of the T4 and T6 tempers is different even in the same alloy (see Fig. 11b). Closure levels are greater in the T6 temper than in the T4 temper for both PM and IM alloys. Under the same applied stress intensity range (ΔK), the magnitude of the crack closure intensity (K_{cl}) is in the order T6-IM > T6-PM > T4-IM > T4-PM. Fig. 11a and b indicates that a higher fatigue crack growth resistance is associated with a higher crack closure of the same alloy. Plasticity induced closure and microroughness induced closure probably existed together here and interacted in a complex manner. The latter is enhanced by a larger grain size [35,36]. This explains the fact that under the same temper, the IM alloy always exhibits a higher degree of crack closure than the PM. It is also well known that microroughness induced closure is mainly significant at

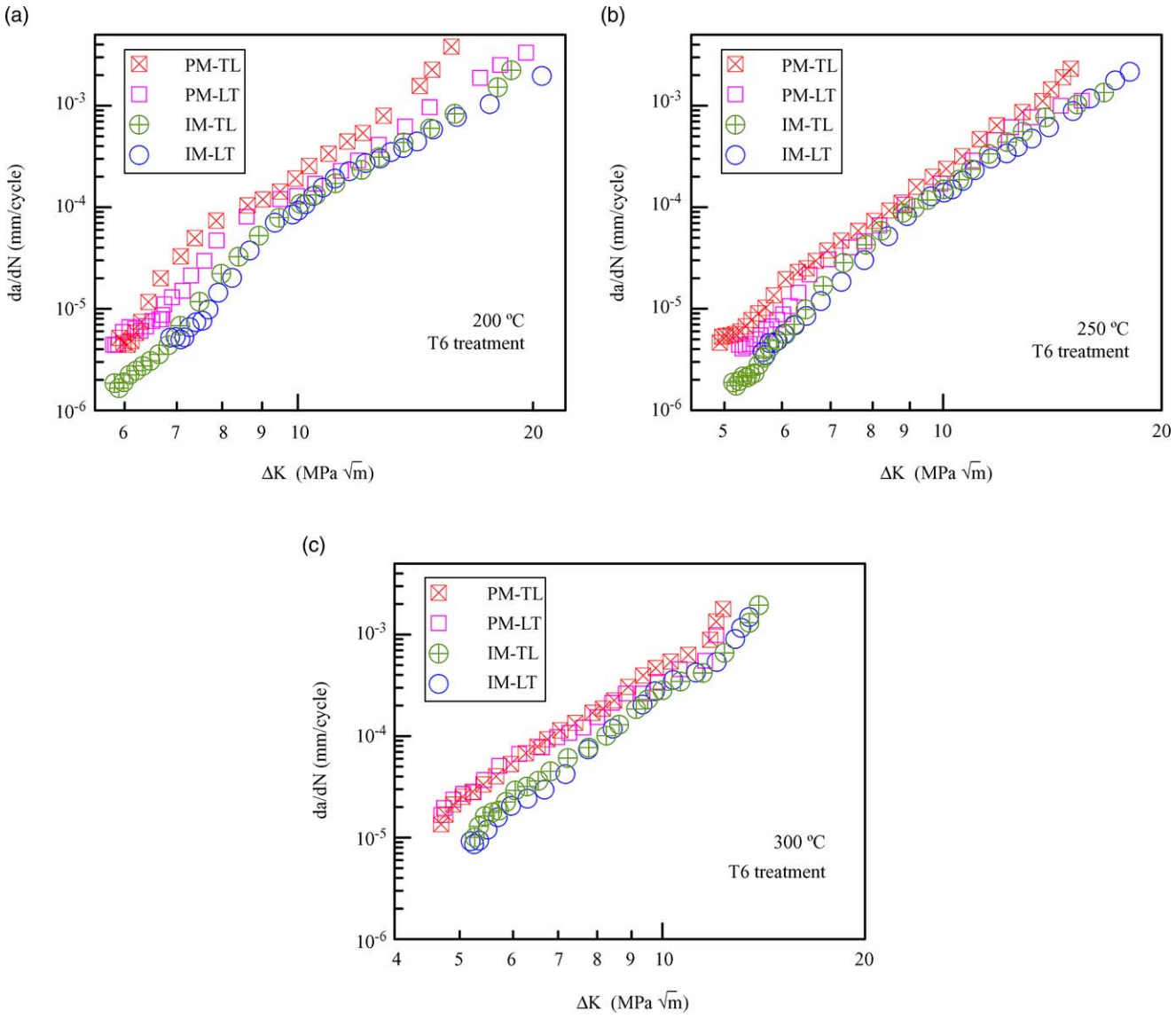

Fig. 10. Comparison of da/dN versus ΔK for the IM and PM alloys in both the LT and TL orientations under the T6 treatment at (a) 200 °C, (b) 250 °C and (c) 300 °C conditions.

low ΔK levels where the crack opening displacements are small. In Fig. 11b, it can be seen that at higher ΔK levels, both the PM and IM alloys of the same temper tend to have similar closure levels. The above comparisons were made on the specimens with the LT orientation. The same observations apply in the TL orientations. T6-IM exhibited an extremely high crack closure intensity of 6.5 MPa$\sqrt{\text{m}}$ at an applied ΔK of 10 MPa$\sqrt{\text{m}}$. Ishii et al. [37] also recorded a rather high crack closure intensity in their T6-IM-6061 alloys of 4.5 MPa$\sqrt{\text{m}}$ at a ΔK of 10 MPa$\sqrt{\text{m}}$. Their specimen thickness was double that used in the current work and their grain size was 6–30 μm, much smaller than the current 200–300 μm. With a larger grain size, the degree of microroughness induced closure will be larger and the current crack closure intensity level is justified.

Crack growth rates are correlated in terms of the effective stress intensity range $\Delta K_{\text{eff}}(=K_{\max}-K_{\text{cl}})$ in Fig. 11c. It is clear that crack closure alone cannot normalize the growth rates in different alloys and tempers. Other microstructure related mechanisms must have played an important role in affecting the fatigue crack growth resistance.

Fig. 12 compares the fracture surface at 25 °C between the IM and PM alloys. Initially, crack growth occurred on a plane perpendicular to the loading direction. At higher ΔK, side edge of cracks started to grow on the 45° slant surface and the crack closure K_{cl} started to decrease. As the ΔK increased near the fast tensile fracture, heavy necking through the specimen thickness occurred in the T4 temper. At the positions where slant fracture and heavy necking started to occur

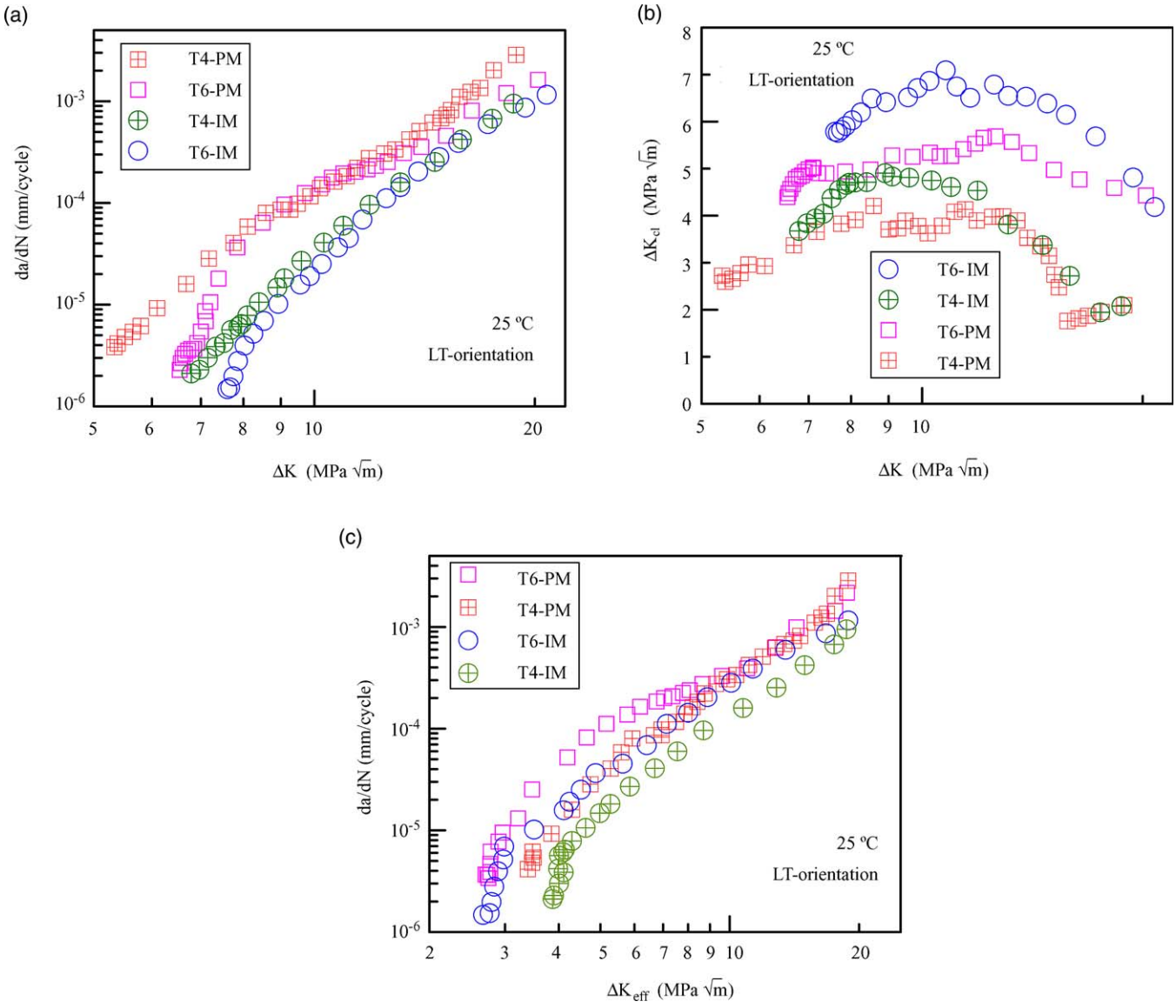

Fig. 11. Comparison of (a) da/dN versus ΔK, (b) crack closure intensity versus ΔK and (c) da/dN versus ΔK_{eff} of the IM and PM alloys under the T4 and T6 heat treatments in the LT orientation.

in the T4 temper specimens, the remaining ligaments were less than the $4/\pi(K_{\max}/\sigma_y)^2$ requirement of ASTM E647. However, the remaining ligaments in the range of ΔK presented were still valid for both PM and IM alloys in T6 temper. At low stress intensity level, the fracture surface of the IM alloy is full of ridges and facets [38] with facet sizes of the order of the grain size. As the stress intensity becomes higher than 8 MPa$\sqrt{\text{m}}$, the microroughness of the fracture surface decreased. Striations are evident under different stress intensities. For the PM alloy, striations were slightly difficult to discern. The fracture surface was comparably smoother than that of the IM alloy even at low stress intensities. This may be related to the observation that the IM alloy has a higher degree of crack closure than the PM alloy under the same heat treatment and stress intensity conditions.

3.2.3. *Effect of temperature*

A comparison of Figs. 9b and 10a–c showed that as temperature was increased from 25 to 300 °C, the difference between fatigue crack growth resistance in PM and IM alloys initially decreased but increased again beyond 250 °C. The fatigue crack growth data at different temperature were collected together in Fig. 13. As expected, for a given alloy fatigue crack growth rate increased with temperature. This increase was more marked at lower ΔK. Also, the increase was more prominent from 25 to 200 °C and also from 250 to 300 °C. The increase from 200 to 250 °C was not so

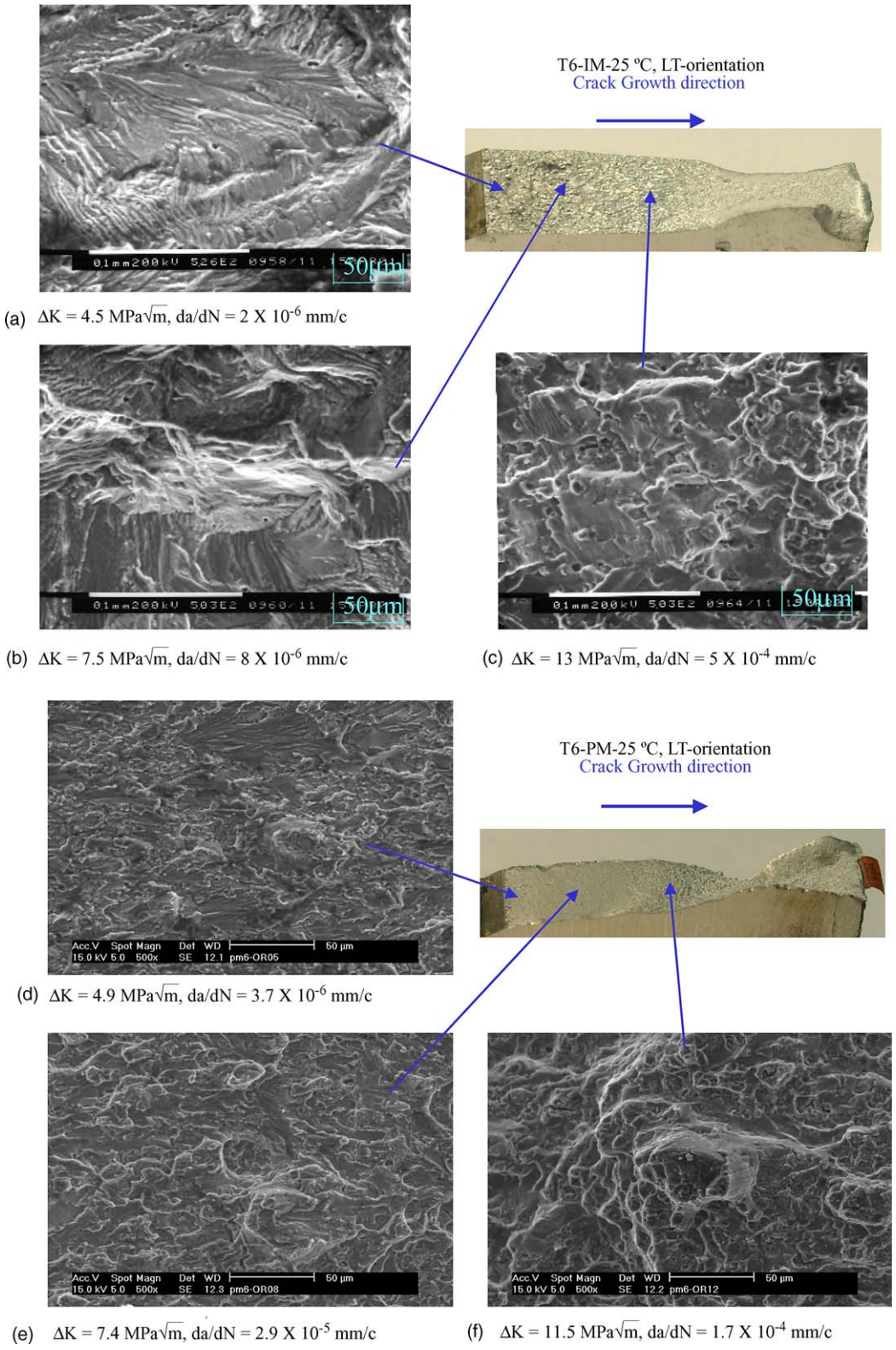

Fig. 12. Room temperature fatigue fracture surfaces in LT-orientation for T6-IM alloy at (a) $U = 0.52$, (b) $U = 0.42$, (c) $U = 0.78$ and T6-PM alloy (d) $U = 0.45$, (e) $U = 0.66$, (f) $U = 0.83$.

marked. At all temperatures examined, the PM alloy always has an inferior fatigue crack growth resistance than the IM alloy. Below 300 °C, the latter difference was so prominent that the crack growth rates of IM at 200 and 250 °C are lower than that of PM at 25 and 200 °C, respectively. However, since there is a sharp

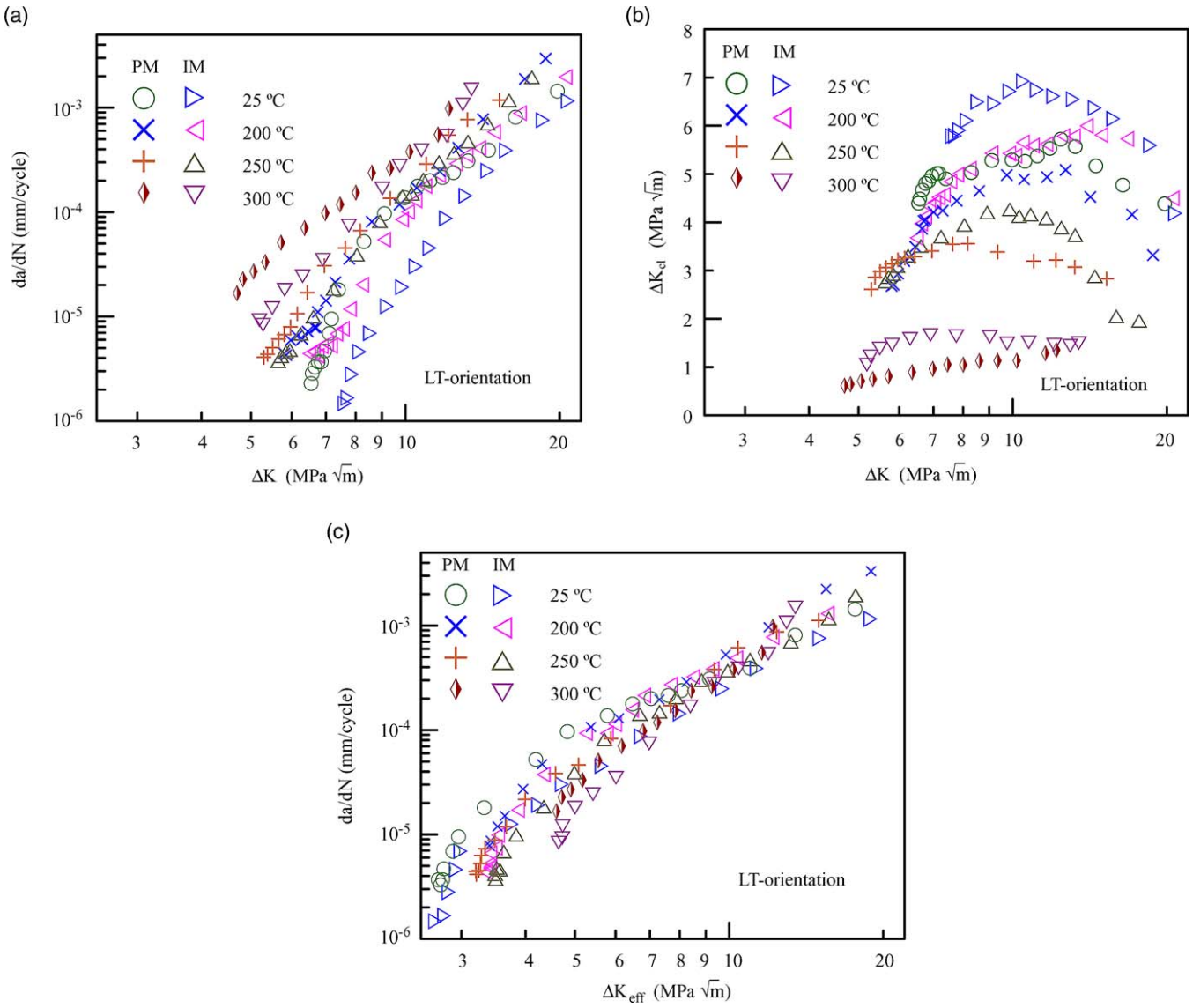

Fig. 13. Comparison of (a) da/dN versus ΔK, (b) crack closure intensity versus ΔK and (c) da/dN versus ΔK_{eff} of the IM and PM alloys at 25, 200, 250 and 300 °C under the T6 heat treatments in the LT orientation.

increase in growth rate from 250 to 300 °C, the 300 °C crack growth rate of the IM alloy is higher than that of 250 °C PM rate.

Fig. 13b compares the development of crack closure intensities at different temperatures for the IM and PM T6 alloys. The alloys exhibited larger than 15% and 55% drop in yield strength at 200 and 300 °C, respectively, while the moduli were also decreased with increasing temperature. These would promote crack tip opening and blunting, resulting in a decreasing degree of crack closure. The difference in the amount of closure between IM and PM alloy at the same temperature may be attributed to their difference in grain size. The larger grain size IM alloy always exhibited more closure than the PM alloy under the same condition. In fact, at 300 °C PM alloy data showed virtually no crack closure throughout, but the 300 °C IM alloy data did show crack closure at the low and medium stress intensity ranges. Unlike the relative change in crack growth resistance with temperature, the decrease in the degree of crack closure is equally prominent from 200 to 250 °C and from 250 to 300 °C. Comparing Fig. 13a and b indicates that a higher fatigue crack growth resistance is associated with a higher crack closure.

Fig. 13c shows the fatigue crack growth rate correlated in terms of the effective stress intensity range ΔK_{eff}. At 200 °C and above, the growth behaviors of the IM and PM alloys under the same temperature fall onto the same curve. At 25 °C, ΔK_{eff} brings the IM and PM growth rate together for $\Delta K_{\text{eff}} \leq 3.5$ MPa$\sqrt{\text{m}}$ and above 9 MPa$\sqrt{\text{m}}$. In between, the PM alloy still grew with a higher rate than the IM alloy under the same

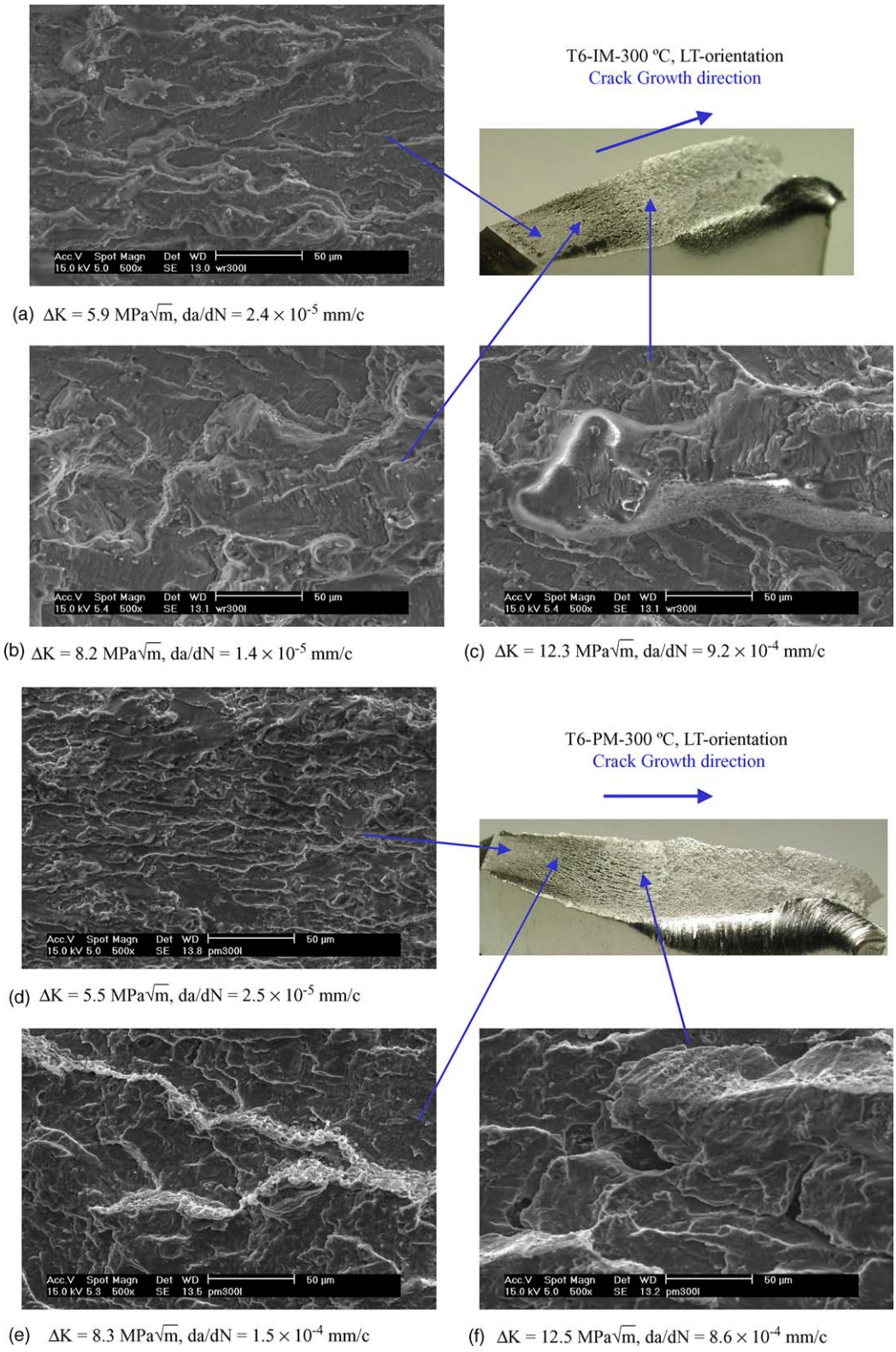

Fig. 14. Fatigue fracture surfaces at 300 °C of T6-IM alloy (a) $U = 0.82$, (b) $U = 0.78$, (c) $U = 1.0$ and T6-PM alloy (d) $U = 0.97$, (e) $U = 0.98$, (f) $U = 1.0$.

ΔK_{eff}. Failure of ΔK_{eff} to bring all the IM and PM growth rate in line suggests that the microstructural influence such as difference in precipitation morphology may also have a significant effect on the fatigue crack growth resistance. At elevated temperatures, lowering of yield strength and change in microstruc-

tural morphology will tend to make such influence subside and so the IM and PM data are brought in line by taking into account of crack closure. Intergranular cracking failure was noticeable at higher values of ΔK and temperatures. Fig. 13c also showed that above ΔK_{eff} of 8 MPa$\sqrt{\text{m}}$, the crack growth data for both alloys tested at the different temperatures were brought into a narrow scatter band if correlated in terms of ΔK_{eff}. At lower ΔK_{eff}, the crack growth rate was the fastest rate at 25 °C, while the slowest at 300 °C. The 200 and 250 °C data fall close together in a band that lies intermediate between the 25 and 300 °C data. It is interesting to note that when correlated in terms of ΔK_{eff}, the fatigue crack growth rates at lower temperatures are in fact faster than that at higher temperatures. One possible reason to this phenomenon is that crack tip blunting occurred so heavily at 300 °C that the stress intensity ranges ΔK and ΔK_{eff}, which are defined for a sharp cracks, may have over-estimated the crack driving forces. The phenomenon is masked by serious difference in crack closure when growth rates are correlated in terms of ΔK but becomes evident under ΔK_{eff}.

Fig. 14 compares the fracture surfaces at 300 °C. Striations are again easily seen on the IM fracture surface but not on the PM fracture surface. The microroughness (observed from the SEM) of the IM alloy is much smaller than that at 25 °C. The microroughness of both alloy is comparable. At high stress intensity, secondary cracks are evident and more marked in the PM alloy.

The above comparison shows that the PM alloy is inferior to the IM alloy in FCP resistance. One possible way to improve this is to add reinforcement such as SiC to reinforce the aluminum-based metal. Work in this direction is currently going on in our laboratory.

4. Conclusions

A study of the tensile and fatigue crack growth properties of 6061 Al alloy fabricated by IM and PM routes has been evaluated at temperatures ranging from 25 to 300 °C. The conclusions are as follows:

1. At 25 °C, the PM alloy possesses a higher strength, higher strain hardening rate and a lower elongation than the IM alloy. Presumably, this is due to the smaller grain size of the former.
2. Raising the testing temperature from 25 to 200 °C greatly reduced the strength of the PM alloy over that of the IM alloy. At 300 °C, both alloys possess similar strength. Raising temperature increases the elongation of the PM alloy. For the IM alloy, elongation increases when temperature is raised from 25 to 200 °C, however, further increase to 300 °C causes the elongation to drop below that at 25 °C.
3. In both IM and PM alloys under both T4 and T6 tempers, the fatigue crack growth resistance in the TL orientation is inferior to that in the LT orientation. The difference in resistance is evident at low stress intensity in the IM alloy and is believed to be resulted from the interaction between grain size and plastic zone size, and at high stress intensity in the PM alloy which is attributable to the difference in fracture toughness. Difference in crack growth resistance between the two orientations decreases with temperature and is basically non-existent at 300 °C.
4. In both PM and IM alloys, the fatigue crack growth resistance in the T6 temper is superior to that in the T4 temper. However, the difference was significant at and below a stress intensity of 8 MPa$\sqrt{\text{m}}$. Moreover, such difference is less prominent than the difference in crack growth resistance between the alloys from the PM and IM routes.
5. In both alloys, fatigue crack growth resistance decreases with temperature. Such decrease is more prominent from 25 to 200 °C and from 250 to 300 °C. The decrease from 200 to 250 °C is not so marked.
6. At all temperatures, the PM alloy always has an inferior crack growth resistance than the IM alloy. However, the difference decreases from 25 to 250 °C, it then increases again from 250 to 300 °C. At temperature at or above 200 °C, the crack growth rate of both alloys can be brought into a narrow scatter band when correlated in terms of ΔK_{eff}. At 25 °C, ΔK_{eff} is unsuccessful in bringing the growth rates from both alloys in line when ΔK_{eff} is smaller than 3.5 MPa$\sqrt{\text{m}}$ or larger than 9 MPa$\sqrt{\text{m}}$.

References

[1] Miller WS, Zhuang L, Bottema J, Wittebrood AJ, De Smet P, Haszler A, et al. Recent development in aluminum alloys for the automotive industry. Materials Science and Engineering 2000;A280:37–49.
[2] Engler O, Hirsch J. Texture control by thermomechanical processing of AA 6xxx Al–Mg–Si sheet alloys for automotive applications—a review. Materials Science and Engineering 2002;A336:249–62.
[3] Srivatsan TS, Sriram S, Daniels C. Influence of temperature on cyclic stress response and fracture behavior of aluminum alloy 6061. Engineering Fracture Mechanics 1997;56(4):531–50.
[4] Srivatsan TS, Anand S, Narendra N. Mechanisms governing deformation and damage during elevated-temperature fatigue of an aluminum–magnesium–silicon alloy. Journal of Materials Engineering and Performance 1997;6:187–98.
[5] Srivatsan TS. Mechanisms governing cyclic deformation and failure during elevated temperature fatigue of aluminum alloy 7055. International Journal of Fatigue 1999;21:557–69.
[6] Seidman DN, Marquis EA, Dunand DC. Precipitation strengthening at ambient and elevated temperatures of heat-treatable Al(Sc) alloys. Acta Materialia 2002;50:4021–35.

[7] Allison JE, Cole GS. Metal-matrix composites in the automotive industry: opportunities and challenges. JOM 1993;1:19–25.
[8] Mckimpson MG, Pohlenz EL, Thompson SR. Evaluating the mechanical properties of commercial DRA. JOM 1993;1:26–9.
[9] Lloyd DJ. Particle reinforced aluminum and magnesium matrix composites. International Materials Reviews 1994;39(1):1–23.
[10] Nair SV, Tien JK, Bates RC. SiC-reinforced aluminum metal matrix composites. International Materials Reviews 1985;30(6): 275–90.
[11] Chawla KK, Liaw PK, Fishman SG. High-performance composites: commonalty of phenomena. JOM 1996;2:43–4.
[12] Pete Scala E. A brief history of composites in the U.S.—the dream and the success. JOM 1996;2:45–8.
[13] Christophe GE, Isaac MJA, Clark JP. MMCs for automotive engine applications. JOM 1996;2:49–51.
[14] Srivatsan TS, Al-Hajri M, Petraroli M, Hotton B, Lam PC. Influence of silicon carbide particulate reinforcement on quasi static and cyclic fatigue fracture behavior of 6061 aluminum alloy composites. Materials Science and Engineering 2002;A235:202–14.
[15] Han NL, Wang ZG, Wang WL, Zhang GD, Shi CX. Low-cycle fatigue behavior of a particulate SiC/2024 composite at ambient and elevated temperature. Composites Science and Technology 1999;59:147–55.
[16] Martin A, Rodriguez J, Llorca J. Temperature effects on the wear behavior of particulate reinforced Al-based composites. Wear 1999;225-229:615–20.
[17] Nieh TG, Lesuer DR, Syn CK. Tensile and fatigue properties of a 25 vol% SiC particulate reinforced 6090 Al composite at 300 °C. Scripta Metallurgica et Materialia 1995;32(5):707–12.
[18] Mckimpson MG, Scott TE. Processing and properties of metal matrix composites containing discontinuous reinforcement. Materials Science and Engineering 1989;A107:93–106.
[19] Blankenship Jr CP, Kaisand LR. Elevated temperature fatigue crack propagation behavior of an Al–Li–Cu–Mg–Ag–Zr alloy. Scripta Materialia 1996;34(9):1455–60.
[20] Reynols AP. Elevated temperature fatigue of P/M aluminum alloy 8009. Scripta Metallurgica et Materialia 1993;28:201–6.
[21] Gary Bray H. Fatigue crack propagation in dispersion-strengthened P/M aluminum alloys at room and elevated temperatures. P/M in aerospace and defense technologies. 1991, p. 381–92.
[22] Andersen SJ, Zandbergen HW, Jansen J, Traeholt C, Tundal U, Reiso O. The crystal structure of the β″ phase in Al–Mg–Si alloys. Acta Materialia 1998;46(9):3283–98.
[23] Papazian JM. Effect of SiC whiskers and particles on precipitation in aluminum matrix composites. Metallurgical Transactions A 1988;19A:2945–53.
[24] Dutta I, Allen SM. A calorimetric study of precipitation in commercial aluminum alloy 6061. Journal of Materials Science Letters 1991;10:323–6.
[25] Healy JC, Beevers CJ. Fatigue crack propagation in a particulate-reinforced metal-matrix composite at room and elevated temperature. Proceedings of the International Conference on Advanced Composite Materials, 1993. p. 1161–1168.
[26] Tanaka T, Nakayama H, Kobayashi Y. Fatigue crack growth mechanism of MMC at room and higher temperatures. Computer Aided Assessment and Control of Localized Damage—Proceedings of the International Conference, 1996. p. 247–54.
[27] McQueen HJ, Celliers OC. Application of hot workability studies to extrusion processing. Part III: physical and mechanical metallurgy of Al–Mg–Si and Al–Zn–Mg alloys. Canadian Metallurgical Quarterly 1997;36(2):73–86.
[28] McQueen HJ. Substructural influence in the hot rolling of Al alloys. JOM 1998;June:28–33.
[29] Evangelista E, Forcellese A, Gabrielli F, Mengucci P. Hot formability of AA 6061 PM aluminum alloy. Journal of Materials Processing Technology 1990;24:323–32.
[30] Agarwal H, Gokhale AM, Graham S, Horstemeyer MF. Void growth in 6061-aluminum alloy under triaxial stress state. Materials Science and Engineering 2003;A341:35–42.
[31] Baxter WJ, Mckinney TR. Growth of slip bands during fatigue of 6061-T6 aluminum. Metallurgical Transactions A 1988;19: 83–91.
[32] Liu G, Zhang GJ, Ding XD, Sun J, Chen KH. Modeling the strengthening response to aging process of heat-treatable aluminum alloys containing plate/disc- or rod/needle-shaped precipitates. Materials Science and Engineering 2003;A344: 113–24.
[33] Ber LB. Accelerated artificial aging regimes of commercial aluminum alloys. II: Al–Cu, Al–Zn–Mg–(Cu), Al–Mg–Si–(Cu) alloys. Materials Science and Engineering 2000;A280:91–6.
[34] Irwin GR. Plastic zone near a crack and fracture toughness. Proceedings of the Seventh Sagamore Research Conference, 1960. p. 4–13.
[35] Lal DN. A model for the combined effects of stress ratio and grain size on the LEFM fatigue threshold condition. Fatigue and Fracture of Engineering Materials and Structures 1992;15(8): 775–792.
[36] Carter RD, Lee EW, Starke Jr EA, Beevers CJ. The effect of microstructure and environment on fatigue crack closure of 7475 aluminum alloy. Metallurgical Transactions 1984;15A: 555–63.
[37] Ishii H, Tohgo K, Araki H. Fatigue crack propagation of SiC whisker reinforced 6061 aluminum alloy composite. Engineering Fracture Mechanics 1991;40(4/5):821–7.
[38] Llorca J, Ruiz J, Healy JC, Elices M, Beevers CJ. Fatigue crack propagation in salt water, air and high vacuum in a spray-formed particulate-reinforced metal matrix composite. Materials Science and Engineering 1994;A185:1–15.